NUMERICAL SIMULATION OF SPRING REVERBERATION

Stefan Bilbao, *

Acoustics and Audio Group
University of Edinburgh
Edinburgh, UK
sbilbao@staffmail.ed.ac.uk

ABSTRACT

Virtual analog modeling of spring reverberation presents a challenging problem to the algorithm designer, regardless of the particular strategy employed. The difficulties lie in the behaviour of the helical spring, which, due to its inherent curvature, shows characteristics of both coherent and dispersive wave propagation. Though it is possible to emulate such effects in an efficient manner using audio signal processing constructs such as delay lines (for coherent wave propagation) and chains of allpass filters (for dispersive wave propagation), another approach is to make use of direct numerical simulation techniques, such as the finite difference time domain method (FDTD) in order to solve the equations of motion directly. Such an approach, though more computationally intensive, allows a closer link with the underlying model system—and yet, there are severe numerical difficulties associated with such designs, and in particular anomalous numerical dispersion, requiring some care at the design stage. In this paper, a complete model of helical spring vibration is presented; dispersion analysis from an audio perspective allows for model simplification. A detailed description of novel FDTD designs follows, with special attention is paid to issues such as numerical stability, loss modeling, numerical boundary conditions, and computational complexity. Simulation results are presented.

1. INTRODUCTION

Virtual analog modeling, for electronic effects and synthesis modules has seen an enormous amount of work in recent years [1]. Somewhat less investigated has been the case of electromechanical effects, especially when the mechanical components involved have a distributed character (i.e., they cannot be modelled as lumped). Prime examples are plate reverberation, and the system of interest in this paper, spring reverberation [2, 3, 4].

Part of the difficulty in adequately simulating spring reverberation lies in the complexity of the model of a helical spring which, even in the linear case, possesses features which are very much unlike those of what might seem to be similar systems in musical acoustics, such as the string, or ideal bar. See [5, 6, 7, 8] for presentations of the dynamical system governing spring vibration. Helical structures, due to their inherent curvature possess the characteristics of both coherent wave propagation, giving rise to discrete echoes, and dispersive wave propagation, giving the response a diffuse character as well. Nevertheless, modeling of spring reverberation has proceeded apace, with simulation methods based on allpass networks [9, 10, 11], and, for simplified models, through standard time stepping procedures such as finite difference schemes [12].

A model of spring vibration is presented in Section 2, accompanied by dispersion analysis, illustrating regions of coherent and dispersive wave propagation. Finite difference schemes are introduced in Section 3, and simulation results and performance analysis are presented in Section 4.

2. HELICAL SPRING MODELS

A helical structure of the type found in typical spring reverberation units, is characterized by its geometrical parameters as illustrated at left in Figure 1, and namely: R, the coil radius in m, r, the wire diameter in m, α, the pitch angle, and L, the unwound spring length in m. Also necessary are parameters describing the material, namely E, Young's modulus in Pa, ν, Poisson's ratio, and ρ the material density in kg/m^3. A general model of the linear dynamics of such helical structures is due to Wittrick [5, 6] and is most easily written in terms of time t and a curved coordinate s along the axis of the spring (see Figure 1 at right) as a system of 12 variables:

$$\partial_s \boldsymbol{\xi} = \frac{\cos^2(\alpha)}{R}\mathbf{J}\boldsymbol{\xi} + \mathbf{E}\boldsymbol{\theta} + \frac{1}{GA\gamma}\mathbf{K}\mathbf{p} \tag{1a}$$

$$\partial_s \boldsymbol{\theta} = \frac{\cos^2(\alpha)}{R}\mathbf{J}\boldsymbol{\theta} + \frac{1}{EI}\mathbf{L}\mathbf{m} \tag{1b}$$

$$\partial_s \mathbf{m} = \frac{\cos^2(\alpha)}{R}\mathbf{J}\mathbf{m} + \mathbf{E}\mathbf{p} + \rho I \mathbf{M}\partial_{tt}\boldsymbol{\theta} \tag{1c}$$

$$\partial_s \mathbf{p} = \frac{\cos^2(\alpha)}{R}\mathbf{J}\mathbf{p} + \rho A \partial_{tt}\boldsymbol{\xi} \tag{1d}$$

Here, the vector variables $\boldsymbol{\xi}$, $\boldsymbol{\theta}$, $\mathbf{m}$ and $\mathbf{p}$,

$$\boldsymbol{\xi} = \begin{bmatrix} u \\ v \\ w \end{bmatrix} \quad \boldsymbol{\theta} = \begin{bmatrix} \theta_u \\ \theta_v \\ \theta_w \end{bmatrix} \quad \mathbf{m} = \begin{bmatrix} m_u \\ m_v \\ m_w \end{bmatrix} \quad \mathbf{p} = \begin{bmatrix} p_u \\ p_v \\ p_w \end{bmatrix} \tag{2}$$

represent, respectively, displacements, rotation angles, moments and forces relative to orthogonal local coordinates $(\gamma_u, \gamma_v, \gamma_w)$ at location s along the spring axis. $A = \pi r^2$ is the cross sectional area of the spring, and ∂_s and ∂_t represent partial differentiation with respect to the coordinates s and t, respectively (and $\partial_{tt} = \partial_t^2$). The system matrices $\mathbf{J}$ and $\mathbf{E}$ are given by

$$\mathbf{J} = \begin{bmatrix} 0 & \tan(\alpha) & -1 \\ -\tan(\alpha) & 0 & 0 \\ 1 & 0 & 0 \end{bmatrix} \quad \mathbf{E} = \begin{bmatrix} 0 & 1 & 0 \\ -1 & 0 & 0 \\ 0 & 0 & 0 \end{bmatrix} \tag{3}$$

* This work was supported by the European Research Council, under grant StG-2011-279068-NESS.

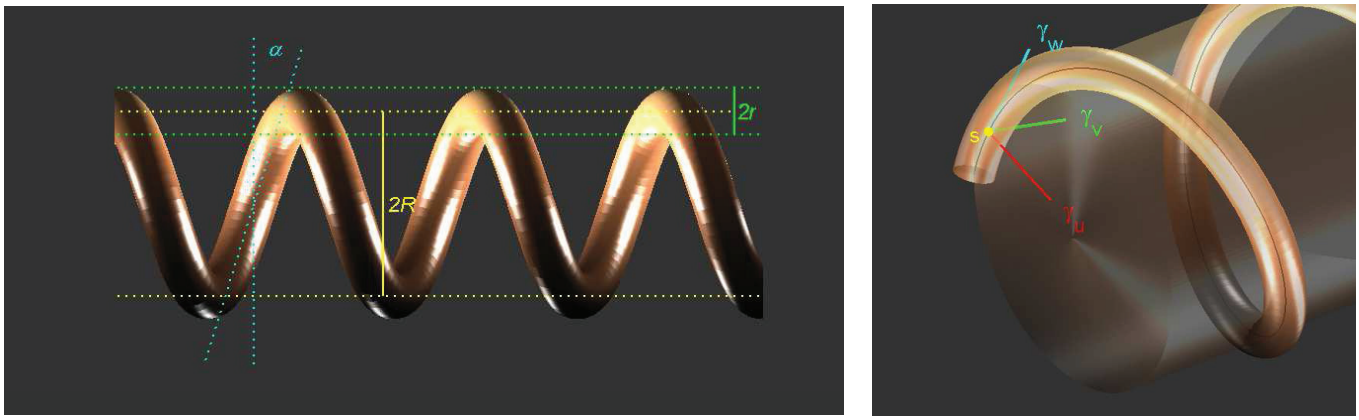

Figure 1: *A helical spring. Left, side view illustrating the coil radius R, wire radius r and pitch angle α. Right, view illustrating the orthogonal coordinates $[\gamma_u, \gamma_v, \gamma_w]$ at curvilinear coordinate s along the spring wire axis.*

and $\mathbf{K}$, $\mathbf{L}$ and $\mathbf{M}$ are diagonal matrices given by

$$\mathbf{K} = \begin{bmatrix} 1 & 0 & 0 \\ 0 & 1 & 0 \\ 0 & 0 & \frac{G\gamma}{E} \end{bmatrix} \mathbf{L} = \begin{bmatrix} 1 & 0 & 0 \\ 0 & 1 & 0 \\ 0 & 0 & \frac{EI}{GI_\phi} \end{bmatrix} \mathbf{M} = \begin{bmatrix} 1 & 0 & 0 \\ 0 & 1 & 0 \\ 0 & 0 & \frac{I_\phi}{I} \end{bmatrix} \tag{4}$$

where $G = E/2(1+\nu)$ is the shear modulus, γ is a shear area correction, and where I and I_ϕ are transverse and polar moments of inertia, respectively. For a spring of circular cross section, $\gamma = 0.88$, $I = \pi r^4/4$, and $I_\phi = 2I = \pi r^4/2$.

2.1. Scaled Form

In nondimensional form, i.e., introducing

$$s' = \frac{s}{s_0} \quad t' = \frac{t}{t_0} \quad \boldsymbol{\xi}' = \frac{\boldsymbol{\xi}}{s_0} \quad \boldsymbol{\theta}' = \boldsymbol{\theta} \quad \mathbf{p}' = \frac{s_0^2 \mathbf{p}}{EI} \quad \mathbf{m}' = \frac{s_0 \mathbf{m}}{EI} \tag{5}$$

where $s_0 = R/\cos^2(\alpha)$ and $t_0 = \sqrt{\rho A/EI} R^2/\cos^4(\alpha)$ yields the scaled system (after removing primes):

$$\partial_s \boldsymbol{\xi} = \mathbf{J}\boldsymbol{\xi} + \mathbf{E}\boldsymbol{\theta} + \frac{EI}{GA\gamma s_0^2}\mathbf{K}\mathbf{p} \tag{6a}$$

$$\partial_s \boldsymbol{\theta} = \mathbf{J}\boldsymbol{\theta} + \mathbf{L}\mathbf{m} \tag{6b}$$

$$\partial_s \mathbf{m} = \mathbf{J}\mathbf{m} + \mathbf{E}\mathbf{p} + \frac{I}{As_0^2}\mathbf{M}\partial_{tt}\boldsymbol{\theta} \tag{6c}$$

$$\partial_s \mathbf{p} = \mathbf{J}\mathbf{p} + \partial_{tt}\boldsymbol{\xi} \tag{6d}$$

This model is quite refined, and can be classified as thick—indeed it reduces to the thick model of beam vibration, due to Timoshenko [13], in the limit of vanishing curvature.

2.2. Reduction to a Thin Model

The model described in the previous sections is a complete description of the linear vibration of a helical spring; for audio rate simulation of spring reverberation, however, it is unneccesarily complex. To this end, note that the factors I/As_0^2 in (6a) and (6c) are proportional to r^2/R^2, and are thus extremely small for springs typically found in reverberation units. Neglecting these terms leads to the form:

$$\partial_s \boldsymbol{\xi} = \mathbf{J}\boldsymbol{\xi} + \mathbf{E}\boldsymbol{\theta} \qquad \partial_s \boldsymbol{\theta} = \mathbf{J}\boldsymbol{\theta} + \mathbf{L}\mathbf{m} \tag{7a}$$

$$\partial_s \mathbf{m} = \mathbf{J}\mathbf{m} + \mathbf{E}\mathbf{p} \qquad \partial_s \mathbf{p} = \mathbf{J}\mathbf{p} + \partial_{tt}\boldsymbol{\xi} \tag{7b}$$

This system in 12 variables (i.e., in 4 three-vector variables) can be reduced to a system in eight variables, as:

$$\mathbf{A}\partial_t \tilde{\boldsymbol{\zeta}} = \mathbf{Q}^\dagger \tilde{\boldsymbol{p}} \qquad \tilde{\boldsymbol{p}} = \mathbf{Q}\tilde{\boldsymbol{m}} \qquad \mathbf{D}\partial_t \tilde{\boldsymbol{m}} = \mathbf{Q}^\dagger \tilde{\boldsymbol{\phi}} \qquad \tilde{\boldsymbol{\phi}} = \mathbf{Q}\tilde{\boldsymbol{\zeta}} \tag{8}$$

where the reduced variables $\tilde{\boldsymbol{\zeta}}$, $\tilde{\boldsymbol{\phi}}$, $\tilde{\mathbf{m}}$ and $\tilde{\mathbf{p}}$ are defined as

$$\tilde{\boldsymbol{\zeta}} = \partial_t \begin{bmatrix} v \\ w \end{bmatrix} \quad \tilde{\boldsymbol{\phi}} = \partial_t \begin{bmatrix} \theta_u \\ \theta_v \end{bmatrix} \quad \tilde{\mathbf{m}} = \begin{bmatrix} m_v \\ m_w \end{bmatrix} \quad \tilde{\mathbf{p}} = \begin{bmatrix} p_u \\ p_v \end{bmatrix} \tag{9}$$

and where the matrix differential operators $\mathbf{Q}$, $\mathbf{Q}^\dagger$, $\mathbf{A}$, and $\mathbf{D}$ are defined as

$$\mathbf{Q} = \begin{bmatrix} -\partial_s & -\mu\partial_s \\ -\mu & 1+\partial_{ss} \end{bmatrix} \qquad \mathbf{Q}^\dagger = \begin{bmatrix} \mu & \partial_s \\ -1-\partial_{ss} & \mu\partial_s \end{bmatrix} \tag{10}$$

$$\mathbf{A} = \begin{bmatrix} 1 & 0 \\ 0 & 1-\partial_{ss} \end{bmatrix} \qquad \mathbf{D} = \begin{bmatrix} 1 & 0 \\ 0 & b-\partial_{ss} \end{bmatrix} \tag{11}$$

Note that the displacement u may be recovered from the system as $u = \partial_s w$. The scaled system as a whole now depends only on the three parameters μ, b and λ, defined as

$$\mu = \tan(\alpha) \qquad b = \frac{EI}{GI_\phi} \qquad \lambda = L/s0 \tag{12}$$

This system is similar to that presented in [8]; as a prelude to numerical implementation, note that by elimination of $\tilde{\boldsymbol{\phi}}$ and $\tilde{\boldsymbol{p}}$ the system can be rewritten in terms of $\tilde{\boldsymbol{\zeta}}$ and $\tilde{\mathbf{m}}$ as

$$\mathbf{A}\partial_t \tilde{\boldsymbol{\zeta}} = \partial_s \mathbf{R}\tilde{\boldsymbol{m}} \qquad \mathbf{D}\partial_t \tilde{\boldsymbol{m}} = \partial_s \mathbf{R}\tilde{\boldsymbol{\zeta}} \qquad \partial_s \mathbf{R} = \mathbf{Q}^\dagger \mathbf{Q} \tag{13}$$

where $\mathbf{R}$ may be written explicitly as

$$\mathbf{R} = \begin{bmatrix} -2\mu & 1-\mu^2+\partial_{ss} \\ 1-\mu^2+\partial_{ss} & 2\mu\left(1+\partial_{ss}\right) \end{bmatrix} \tag{14}$$

Finally, by elimination of $\tilde{\boldsymbol{m}}$, a system in $\tilde{\boldsymbol{\xi}} = [v\ w]^T$ alone may be written as

$$\mathbf{A}\partial_{tt}\tilde{\boldsymbol{\xi}} = \partial_{ss}\mathbf{R}\mathbf{D}^{-1}\mathbf{R}\tilde{\boldsymbol{\xi}} \tag{15}$$

where here, $\mathbf{D}^{-1}$ is to be interpreted as the inverse of the differential operator $\mathbf{D}$.

2.3. Dispersion Relations

As a justification for the use of the simplified model (8), as opposed to the full model (1), it is useful to examine the two systems assuming wave like solutions—which is appropriate, as both systems are constant coefficient linear systems. To this end, solutions with harmonic time/space dependence $e^{j(\omega t+\beta s)}$ for all components in both cases, where ω is temporal frequency, and β is wavenumber (both nondimensional). Partial differential operators ∂_t and ∂_s thus behave as multiplicative factors, i.e.

$$\partial_t \Longrightarrow j\omega \qquad \partial_s \Longrightarrow j\beta \tag{16}$$

Under this assumption, system (1) reduces to a 12×12 system of equations in ω and β, and thus possesses 12 dispersion relations of the form $\omega(\beta)$; these are generally grouped in pairs (corresponding to leftward and rightward propagation), so there are essentially six independent such relations.

Consider now a spring of dimensions typical to spring reverberation units. As shown in Figure 2, the six dispersion relations for the full system span a large range of frequencies; there are only two, however, which lie comfortably within the audio range, with the other four in the range above 100 kHz. The reduced model (8) very accurately models the two relations in the audio range, as shown in Figure 2. It is safe to use the reduced model under virtually any spring configuration to be found in a reverberation unit.

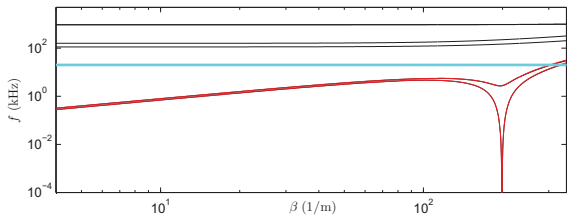

Figure 2: *Log-log plot of dispersion relations $f(\beta)$, in Hz, in dimensional form, for a steel spring of coil radius of $R = 5$ mm, a wire radius of $r = 1$ mm, with a pitch angle of $\alpha = 5°$. Black: the six dispersion relations corresponding to the full model* (1)*, with the upper two indistinguishable in this plot. Red: the two dispersion relations for the reduced system* (8)*. The limit of human hearing at $f = 20$ kHz is indicated by a blue line.*

The two principal dispersion relations of interest possess several general features. See Figure 3 at left, showing such relations for a typical spring under variation in the pitch angle α. Both curves exhibit a main "hump"; the curves track each other closely, but one of the two falls to zero at dimensionless wavenumber $\beta = \sqrt{1+\mu^2}$; this wavenumber corresponds to a wavelength of exactly one full turn of the spring, and at this wavenumber, rigid body rotation (i.e., at frequency $\omega = 0$) is permitted. The second curve shows increasing deviation from the first in this region as the pitch angle α is increased. Above this critical wavenumber, both curves approach those corresponding to dispersive wave propagation in an ideal thin bar.

More useful, from the perceptual standpoint, is the examination of group velocity curves $v_g = d\omega/d\beta$ (see the right panel of Figure 3); flat regions of the curves correspond to coherent wave propagation, and thus to spectral regions over which echoes will be perceived. For more on the interpretation of dispersion relations for the helical spring system, see [14].

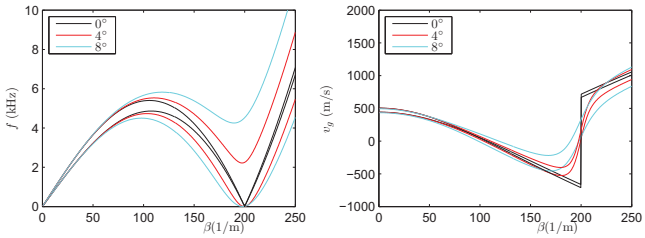

Figure 3: *Left: Principal dispersion relations (dimensional) for the helical spring of parameters given in the caption to Figure 2, under variation in the pitch angle α, as indicated. Right: Associated group velocities v_g.*

2.4. Energy, Boundary Conditions, Forcing and Output

The total energy stored in the spring is a useful quantity in numerical design—see, e.g., [15] for more on this topic. In the present case of a lossless system, it is conserved, provided boundary conditions are chosen as lossless as well.

An energy balance for the system (8) may be written as

$$\frac{d}{dt}\mathcal{H} = \mathcal{B}_{s=\lambda} - \mathcal{B}_{s=0} \tag{17}$$

where the total energy $\mathcal{H}$ is defined as

$$\mathcal{H} = \frac{1}{2}\int_0^\lambda \zeta_v^2 + \zeta_w^2 + (\partial_s \zeta_w)^2 + m_v^2 + b m_w^2 + (\partial_s m_w)^2 \, ds \tag{18}$$

where the first three terms under the integral correspond to kinetic energy density in the three coordinate directions, and the latter three to potential energy. The boundary term consists of six terms:

$$\begin{aligned}\mathcal{B} \;=\; & \zeta_v p_v + \underbrace{(\partial_s \zeta_w)}_{\zeta_u} p_u + \zeta_w \underbrace{(\mu p_v - \partial_s p_u + \partial_s \partial_t \zeta_w)}_{p_w} \\ & + m_v \phi_v + \underbrace{(\partial_s m_w)}_{m_u} \phi_u + m_w \underbrace{(\mu \phi_v - \partial_s \phi_u + b \partial_s \partial_t m_w)}_{\phi_w}\end{aligned} \tag{19}$$

When evaluated at the endpoints of the domain, as in (17), $\mathcal{B}$ has the interpretation of power supplied at the boundaries. Under unforced conditions, if $\mathcal{B} = 0$ at the boundaries, then the system is lossless—i.e., $d\mathcal{H}/dt = 0$. Natural boundary conditions are that one constituent of each of the six products in the boundary term above vanish, generalizing frequently occurring conditions such as free, clamped or simply supported to the case of a helical structure. There are obviously many combinations (4096, in fact, considering that there are 64 possible choices of such natural boundary conditions at each end of the spring)!

The terms in (ζ, p) above correspond to power supplied through forcing along the coordinate directions, and those in (m, ϕ) to power supplied through twisting action about the three coordinate directions. Under forced conditions in a spring reverberation unit, though a combination of linear and rotational forcing is certainly present, the assumption here will be that the forcing occurs through the former mechanism, so that one may specify p_u, p_v or

p_w (through the implicit expression in (19)) as an input signal, and leave the corresponding velocity component unspecified.

A simple means of taking output is by directly reading values of the spring velocity $\tilde{\boldsymbol{\zeta}}$ at the location $s = \lambda$ (or, if working with the simplified system (15) in displacements, their time derivatives, which will scale roughly with observed output signals).

2.5. Losses

The question of losses within the spring, due to viscothermal effects is an important one for reverberation purposes; however, it has not seen any investigation, experimental or otherwise, to the knowledge of this author. A basic three parameter loss model, allowing for uncoupled damping effects is as follows:

$$\mathbf{A}\partial_{tt}\tilde{\boldsymbol{\xi}} = \partial_{ss}\mathbf{R}\mathbf{D}^{-1}\mathbf{R}\tilde{\boldsymbol{\xi}} - \begin{bmatrix}\sigma_v & 0\\ 0 & \sigma_w - \sigma_u\partial_{ss}\end{bmatrix}\partial_t\tilde{\boldsymbol{\xi}} \qquad (20)$$

where $\sigma_u, \sigma_v, \sigma_w \geq 0$ are loss parameters corresponding to vibration in the γ_u, γ_v and γ_w coordinates respectively (and taking into account the relationship between u and w in the reduced form).

3. FINITE DIFFERENCE TIME DOMAIN METHODS

There are several different equivalent systems presented in Section 2; the full model in eight variables (8), a system in four variables (13) and finally a system in two displacements alone (15) (as well as the lossy system (20)). The first is useful in the construction of simulation methods, and in properly modeling boundary conditions; the latter are the forms which are most useful in a practical implementation.

3.1. Grid Functions

In moving to a discrete time formulation, the first step is the choice of sample rate F_s, and the resulting time step $k = 1/F_s$.

First consider system (15), in the displacements $\tilde{\boldsymbol{\xi}}$ alone. A grid spacing h may be chosen, such that $\lambda/h = N$, for integer N, and subject to stability conditions (see Section 3.4). The grid function $\tilde{\boldsymbol{\xi}}_l^n$ then represents an approximation to $\tilde{\boldsymbol{\xi}}(s,t)$ at times $t = nk$, for integer n, and at locations $s = lh$, for $l = 0, \ldots, N$. See Figure 4, showing the lattice of grid point corresponding to $\tilde{\boldsymbol{\xi}}_l^n$ in black.

The system (13) in velocities $\tilde{\boldsymbol{\zeta}}$ and moments $\tilde{\boldsymbol{m}}$ permits an interleaved discretization, similar to that which occurs in FDTD schemes for electromagnetics [16, 17]. One may define the grid functions

$$\tilde{\boldsymbol{\zeta}}_l^{n+\frac{1}{2}} \approxeq \tilde{\boldsymbol{\zeta}}|_{t=(n+\frac{1}{2})k, s=lh} \qquad \tilde{\boldsymbol{m}}_{l+\frac{1}{2}}^{n} \approxeq \tilde{\boldsymbol{m}}|_{t=nk, s=(l+\frac{1}{2})h} \qquad (21)$$

as illustrated by white points in Figure 4. $\tilde{\boldsymbol{\zeta}}_l^{n+\frac{1}{2}}$ is defined for $l = 0, \ldots, N$, and $\tilde{\boldsymbol{m}}_{l+\frac{1}{2}}^{n}$ for $l = 0, \ldots, N-1$.

Finally, for the complete system (8), grid functions corresponding to $\tilde{\boldsymbol{\phi}}$ and $\tilde{\boldsymbol{p}}$ are necessary. It is appropriate, given the structure of system (8), to split the components of these vector variables onto distinct grids as:

$$\tilde{\boldsymbol{\phi}}_{u,l+1/2}^{n+\frac{1}{2}} \qquad \tilde{\boldsymbol{\phi}}_{v,l}^{n+\frac{1}{2}} \qquad \tilde{\boldsymbol{p}}_{u,l}^{n} \qquad \tilde{\boldsymbol{p}}_{v,l+\frac{1}{2}}^{n} \qquad (22)$$

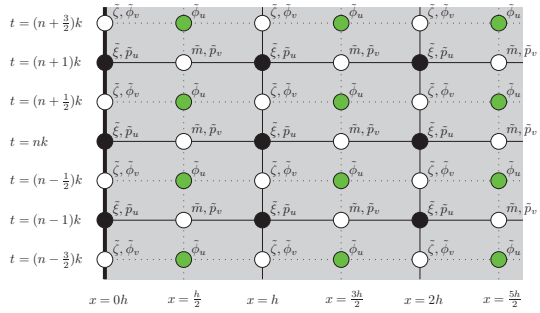

Figure 4: *Computational grids for FDTD schemes for the helical spring. Black points indicate a regular lattice for displacements $\tilde{\boldsymbol{\xi}}_l^n$ and white points indicate an interleaved lattice in velocities $\tilde{\boldsymbol{\zeta}}_l^{n+\frac{1}{2}}$ and moments $\tilde{\boldsymbol{m}}_{l+\frac{1}{2}}^n$. A scheme for the full system requires an additional lattice of points, indicated in green.*

where $\tilde{\boldsymbol{\phi}}_{v,l}^{n+\frac{1}{2}}$ and $\tilde{\boldsymbol{p}}_{u,l}^{n}$ are defined for $l = 0, \ldots, N$, and $\tilde{\boldsymbol{\phi}}_{u,l+1/2}^{n+\frac{1}{2}}$ and $\tilde{\boldsymbol{p}}_{v,l+\frac{1}{2}}^{n}$ for $l = 0 \ldots, N-1$. The lattices of grid points corresponding to these grid functions are as indicated in Figure 4.

3.2. Difference Operators

For a given grid function f_l^n (where here, l and n are either integer or half-integer), forward and backward approximations δ_{t+} and δ_{t-} to the time derivative ∂_t are defined as

$$\delta_{t+}f_l^n = \frac{1}{k}\left(f_l^{n+1} - f_l^n\right) \qquad \delta_{t-}f_l^n = \frac{1}{k}\left(f_l^n - f_l^{n-1}\right) \quad (23)$$

Similarly, forward and backward approximations δ_{s+} and δ_{s-} to the spatial derivative ∂_s are defined as

$$\delta_{s+}f_l^n = \frac{1}{h}\left(f_{l+1}^n - f_l^n\right) \qquad \delta_{s-}f_l^n = \frac{1}{h}\left(f_l^n - f_{l-1}^n\right) \quad (24)$$

Approximations to higher derivatives may be obtained through composition of the above operations. For example, centred approximations to the second time and space derivatives ∂_{tt} and ∂_{ss} may be obtained as the operator products $\delta_{tt} = \delta_{t+}\delta_{t-}$ and $\delta_{ss} = \delta_{s+}\delta_{s-}$.

The main spatial differential operators for the spring system are as given in (10), and may be directly transferred to spatial difference operators as

$$\begin{aligned}\mathbf{Q}_{d,\pm} &= \begin{bmatrix}-\delta_{s\pm} & -\mu\delta_{s\pm}\\ -\mu & 1+\delta_{ss}\end{bmatrix} \qquad \mathbf{Q}_{d,\pm}^{\dagger} = \begin{bmatrix}\mu & \delta_{s\pm}\\ -1-\delta_{ss} & \mu\delta_{s\pm}\end{bmatrix}\\ \mathbf{A}_d &= \begin{bmatrix}1 & 0\\ 0 & 1-\delta_{ss}\end{bmatrix} \qquad \mathbf{D}_d = \begin{bmatrix}1 & 0\\ 0 & b-\delta_{ss}\end{bmatrix}\end{aligned} \qquad (25)$$

Note that due to the interleaved character of the grid functions, the differential operators $\mathbf{Q}$ and $\mathbf{Q}^{\dagger}$ have been replaced by forward and backward difference operations $\mathbf{Q}_{d,\pm}$, and $\mathbf{Q}_{d,\pm}^{\dagger}$ respectively.

If the reduced systems (13) or (15) are to be used, then the difference operator $\mathbf{R}_d$, corresponding to $\mathbf{R}$ may be defined in terms of either of these pairs of operators as

$$\delta_{s\pm}\mathbf{R}_d = \mathbf{Q}_{d,\pm}^{\dagger}\mathbf{Q}_{d,\pm} \qquad (26)$$

and takes the explicit form

$$\mathbf{R}_d = \begin{bmatrix} -2\mu & 1-\mu^2+\delta_{ss} \\ 1-\mu^2+\delta_{ss} & 2\mu(1+\delta_{ss}) \end{bmatrix} \tag{27}$$

3.3. Interleaved Scheme

Assembling the various difference approximations to the operators in (8) leads immediately to the following interleaved form:

$$\begin{aligned} \mathbf{A}_d\delta_{t-}\tilde{\boldsymbol{\zeta}} &= \mathbf{Q}_{d,-}^{\dagger}\tilde{\boldsymbol{p}} \qquad \tilde{\boldsymbol{p}} = \mathbf{Q}_{d,-}\tilde{\boldsymbol{m}} \\ \mathbf{D}_d\delta_{t+}\tilde{\boldsymbol{m}} &= \mathbf{Q}_{d,+}^{\dagger}\tilde{\boldsymbol{\phi}} \qquad \tilde{\boldsymbol{\phi}} = \mathbf{Q}_{d,+}\tilde{\boldsymbol{\zeta}} \end{aligned} \tag{28}$$

Reduced forms corresponding to (13) and (15) can be written as

$$\mathbf{A}_d\delta_{t-}\tilde{\boldsymbol{\zeta}} = \delta_{s-}\mathbf{R}_d\tilde{\boldsymbol{m}} \qquad \mathbf{D}_d\delta_{t+}\tilde{\boldsymbol{m}} = \partial_{s+}\mathbf{R}_d\tilde{\boldsymbol{\zeta}} \tag{29}$$

and

$$\mathbf{A}_d\delta_{tt}\tilde{\boldsymbol{\xi}} = \delta_{ss}\mathbf{R}_d\mathbf{D}_d^{-1}\mathbf{R}_d\tilde{\boldsymbol{\xi}} \tag{30}$$

where as before, $\mathbf{D}_d^{-1}$ is to be interpreted as the inverse of the difference operator $\mathbf{D}_d$ (i.e., in implementation it will become a matrix inversion or linear system solution).

Notice in particular that the single variable scheme in (30) depends only on centered difference operators and is thus second order accurate. All of the above schemes are necessarily implicit, due to the action of the operators $\mathbf{A}_d$ and $\mathbf{D}_d$ (in implementation, these lead to sparse linear system solutions to be carried out at each time step).

3.4. Stability and Numerical Boundary Conditions

The determination of explicit numerical stability conditions for the scheme above is considerably more difficult in the case of the present scheme (or indeed any scheme for this system) than for other related systems (such as, e.g., the ideal string or ideal bar [15]). The difficulty is fundamental: for a given time step k, one would like to find a minimum value h_{min} of the grid spacing such that the scheme does not exhibit explosive growth.

One approach to finding a numerical stability condition is the familiar frequency domain approach due to von Neumann [18]. In this case all grid functions are assumed to exhibit harmonic time/space dependence of the form $e^{j(lh\beta+nk\omega)}$, for angular frequency ω and wavenumber β, and for half integer l and n. Considering, for simplicity, the centred one-variable form (30), the operators δ_{tt} and δ_{ss} transform according to

$$\delta_{tt} \Longrightarrow -\frac{4\sin^2(\omega k/2)}{k^2} \qquad \delta_{ss} \Longrightarrow -\frac{4\sin^2(\beta h/2)}{h^2} \tag{31}$$

and thus the scheme (30) possesses the characteristic equation

$$\sin^2(\omega k/2)\mathbf{I}_2 = \frac{k^2}{h^2}\sin^2(\beta h/2)\hat{\mathbf{A}}_d^{-1}\hat{\mathbf{R}}_d\hat{\mathbf{D}}_d^{-1}\hat{\mathbf{R}}_d \tag{32}$$

where $\mathbf{I}_2$ is the 2×2 identity matrix, and where $\hat{\mathbf{A}}_d$, $\hat{\mathbf{D}}_d$ and $\hat{\mathbf{R}}_d$ are the wavenumber-dependent matrices obtained through replacement of δ_{ss} by the factor $-\frac{4\sin^2(\beta h/2)}{h^2}$ in the definitions (25) and (27). As such, the necessary stability condition follows as

$$\text{eig}\left(\frac{k^2}{h^2}\sin^2(\beta h/2)\hat{\mathbf{A}}_d^{-1}\hat{\mathbf{R}}_d\hat{\mathbf{D}}_d^{-1}\hat{\mathbf{R}}_d\right) \leq 1 \tag{33}$$

for all β with $0 \leq \beta \leq \pi/h$. Ideally, one would like to be able to determine a closed form expression for the minimal grid spacing $h_{min}(k)$, such that the above condition is satisfied for all $h \geq h_{min}(k)$—in audio applications, for best results, for a given time step k, it is best to choose h as close to h_{min} as possible [15]. Unfortunately, such a closed form condition is not available in the present case, and thus h_{min} must be determined numerically.

In the limit of high sample rates (or small time steps), the minimal grid spacing approaches the following bound:

$$\lim_{k\to 0} h_{min}(k) = \sqrt{2k} \tag{34}$$

The square root dependence is typical of schemes for stiff systems such as the ideal bar (indeed, at high frequencies, the helical spring system approaches that of the ideal bar). See, e.g., [15].

Energy conservation methods [19] are a more powerful means of obtaining stability conditions, as proper numerical boundary conditions may also be determined (though the difficulty in obtaining a closed form expression for h_{min} remains). The idea is to obtain an energy balance analogous to (17), such that numerical energy is conserved from one time step to the next—numerical stability then amounts to finding conditions under which the numerical energy is positive semi-definite in the grid functions, allowing solution growth to be bounded.

Though there is not space here to give a full treatment of energy methods, a discrete energy balance can be shown to be:

$$\delta_{t+}\mathcal{H}_d = \mathcal{B}_{d,0} - \mathcal{B}_{d,N} \tag{35}$$

where one expression for $\mathcal{H}_d^n$, the discrete conserved energy at time step n, is

$$\begin{aligned} \mathcal{H}_d^n = \frac{h}{2}\Big(&\sum_{l=0}^{N}{}' \left(\zeta_{v,l}^n\right)^2 + \left(\zeta_{w,l}^n\right)^2 + \sum_{l=0}^{N-1}\frac{1}{h^2}\left(\zeta_{w,l+1}^n - \zeta_{w,l}^n\right)^2 \\ &+ \sum_{l=0}^{N-1} m_{v,l+\frac{1}{2}}^{n+\frac{1}{2}} m_{v,l+\frac{1}{2}}^{n-\frac{1}{2}} + b m_{w,l+\frac{1}{2}}^{n+\frac{1}{2}} m_{w,l+\frac{1}{2}}^{n-\frac{1}{2}} \\ &+ \frac{1}{h^2}\sum_{l=0}^{N}{}' \left(m_{w,l+\frac{1}{2}}^{n+\frac{1}{2}} - m_{w,l-\frac{1}{2}}^{n+\frac{1}{2}}\right)\left(m_{w,l+\frac{1}{2}}^{n-\frac{1}{2}} - m_{w,l-\frac{1}{2}}^{n-\frac{1}{2}}\right)\Big) \end{aligned}$$

where the primed sum indicates a factor of 1/2 applied at $l = 0$ and $l = N$. Such an expression mirrors that in (18), though in this case, the terms in $\tilde{\mathbf{m}}$ are not necessarily positive. The determination of conditions under which the above expression is non-negative as a whole (by relating $\tilde{\mathbf{m}}$ back to $\tilde{\boldsymbol{\zeta}}$ through (29)) is difficult, and amounts to the same problem discussed with reference to frequency domain methods above.

The boundary terms $\mathcal{B}_{d,0}$ and $-\mathcal{B}_{d,N}$ again indicate power supplied at the endpoints of the domain, at $l = 0$ and $l = N$; the expressions are rather lengthy, and will not be included here—the general form, however, is the same as that for the continuous system from (19), and is made up of six products of grid functions evaluated at the boundary. The important point is that one may ensure numerical losslessness, under unforced conditions, by requiring that one member of each of the six pairs vanishes. See Section 4.2. It is important to point out that, in contrast to the continuous case, the expression for the numerical energy $\mathcal{H}_d$ is not unique—each choice leads to a distinct set of numerical boundary conditions.

3.5. Numerical Dispersion

The scheme (28) (or the equivalent reduced forms) for the helical spring exhibits numerical dispersion—i.e., propagation speeds

deviate from those of the model system. Such behaviour may be analyzed through the characteristic equation (32), which possesses two solutions $\omega(\beta)$. See Figure 5, showing numerical dispersion relations at a variety of audio sample rates. The dispersion curves converge (with increasing sample rate) rather slowly to those of the model system. An appeal to more delicate modeling is in order—see Section A for some more involved numerical designs targeting this deficiency.

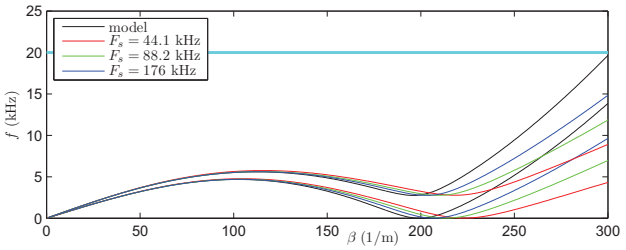

Figure 5: *Numerical dispersion relations, for a variety of audio sample rates, for scheme* (28) *for the helical spring system, for a steel spring of coil radius $R = 5$ mm, wire radius of $r = 1$ mm, and pitch angle $\alpha = 5°$.*

4. SIMULATION RESULTS AND PERFORMANCE ANALYSIS

In this section, some simulation results are presented, for springs of dimensions typically found in reverberation units.

4.1. Response to an Impulsive Excitation

Figure 6 shows snapshots of the time evolution of the state of a helical spring, when subjected to a short impulsive excitation aligned nearly with the coil axis (at right), and transverse to it (at left)—in this case, the values of the forcing function $\tilde{\mathbf{p}}$ in the appropriate direction specified at the boundary at $l = 0$. Note in particular the conversion of the vibrational energy almost instantaneously to vibration in the other coordinate directions.

4.2. Energy Conservation

The scheme (28), as discussed in Section 3.4, conserves energy to machine accuracy under lossless conditions, as long as appropriate conservative boundary conditions are applied. See Figure 7, illustrating the variation in numerical energy for a spring subjected to an impulsive excitation—note that energy is quantized to multiples of machine precision. Such a property, beyond being useful in stability analysis, serves as an excellent debugging tool—any errors in the implementation will almost certainly lead to anomalous variation in the numerical energy. When losses are present, numerical energy, at least under the model will be monotonically decreasing.

4.3. Spring Responses

In this section, spectrograms of simulated spring output responses are shown. In all cases here, the spring is steel, of length $L = 5$ m, with $R = 4$ mm, $r = 0.2$ mm, and with a pitch angle of 1.7°;

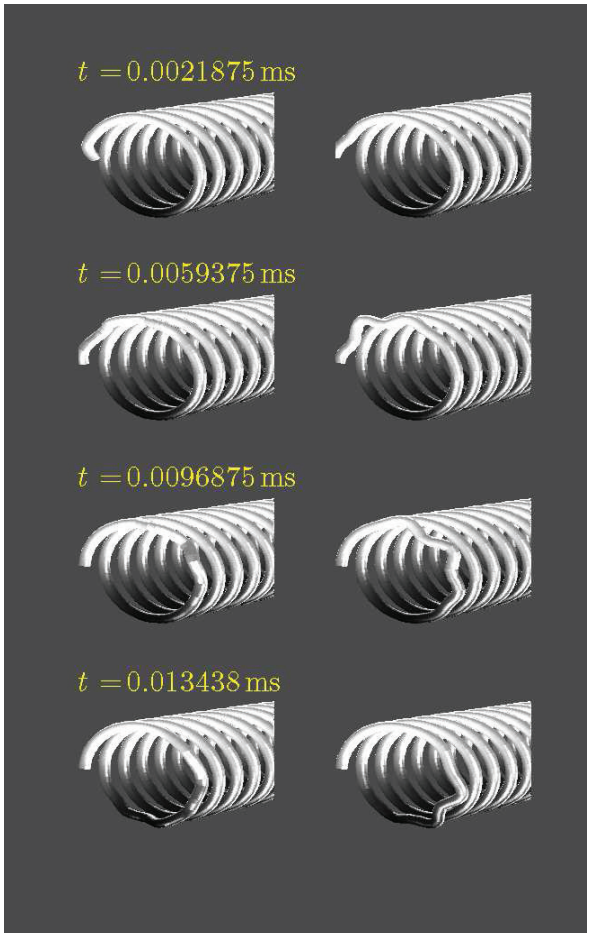

Figure 6: *Snapshots of the time evolution of a helical spring, subject to an impulsive excitation, at times as indicated. The spring is steel, with $R = 4$ mm, and $r = 0.2$ mm and a pitch angle of $\alpha = 5°$. Left: excitation along coordinate direction γ_v. Right: excitation along coordinate direction γ_w. Displacements are exaggerated, for visibility.*

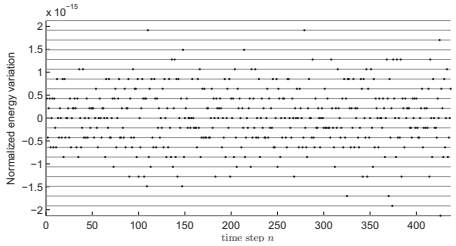

Figure 7: *Numerical energy variation for the spring of parameters as given in the caption to Figure 6, using scheme* (28) *at a sample rate of 44.1 kHz. Multiples of machine epsilon are shown as grey lines.*

output is drawn from velocity ζ_w in the γ_w coordinate direction. Other parameters will be varied here.

The most important consideration, given the discussion of numerical dispersion in Section 3.5, is that of anomalous wave speed,

particularly for echoes. Figure 8 shows spectrograms for spring output under successively larger sample rates. In general, the spectrograms exhibit a complex region, under a cutoff frequency (the frequency at the top of the hump in the plot of the dispersion relation in Figure 3), over which multiple families of dispersive echoes are visible. Above the cutoff, a single family of dispersive chirp-like echoes persists. It is this family which is most affected by numerical dispersion, as should be evident in the plots in Figure 5, and at 44.1 kHz, wave speed is anomalously slow. Thus, unless a scheme with reduced dispersive properties can be devised, such schemes will produce anomalous results at low audio rates (though they may be used at oversampled rates). See Section A for some possible variants on the scheme presented in Section 3.3.

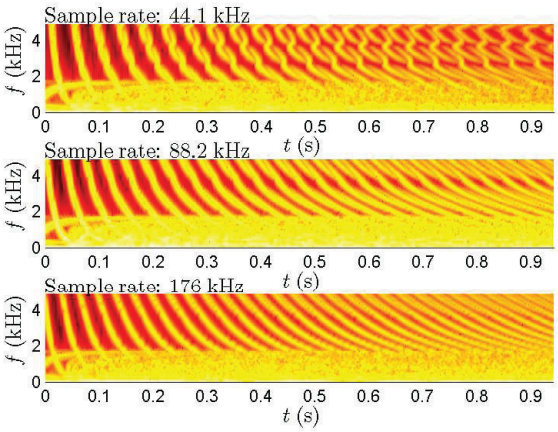

Figure 8: *Spectrograms of output responses, under different choices of the sample rate, as indicated.*

Loss, though discussed only in passing in this article, obviously plays a major role in determining the characteristic sound of a spring reverberation unit. Considering the simple lossy model in (20), it is simple to arrive at a generalization of scheme (30), by replacing instances of ∂_t by a centered approximation $(\delta_{t+} + \delta_{t-})/2$, and ∂_{ss} by δ_{ss}. It is also possible to show that such a perturbation leads to monotonic energy loss.

Consider two cases, as illustrated in Figure 9, selecting for loss along one of the two coordinate directions γ_v or γ_w; as is easily visible, loss along the transverse coordinate γ_v has a much greater effect in terms of energy decay.

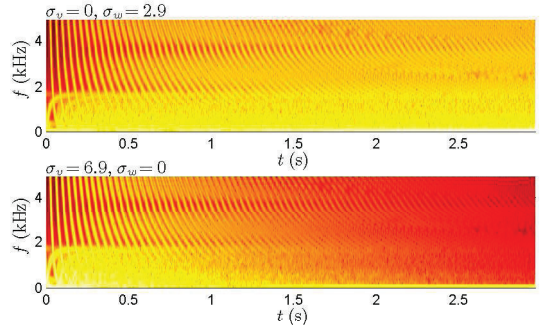

Figure 9: *Spectrograms of output responses, under different choices of loss coefficients σ_v and σ_w, as indicated. The sample rate is 88.2 kHz.*

4.4. Computational Cost

Computational cost for the scheme given in Section 3.3 is high, but not extreme; clearly it depends strongly on the sample rate, so there is some motivation to look for schemes with reduced dispersion—see Section A. As an example, consider a spring of dimensions typical to a reverberation device. In Table 1, simulation times, for one second output are given, for a single core Matlab implementation on a standard laptop computer. Notice in particular that the grid size scales roughly with $\sqrt{F_s}$, and computation time with $F_s^{3/2}$—reflecting the limiting stability condition from (34).

Table 1: Number of grid points N and calculation time, in seconds, for one second output at various sample rates, for a spring with $R = 4$ mm, $r = 0.2$ mm, $L = 5$ m and $\alpha = 1.7°$.

F_s	N	calculation time (s)
44 100	1257	18.13
88 200	1639	50.90
176 000	2205	141.0

5. CONCLUDING REMARKS

A model for a helical spring has been presented here; the continuous model (8) presented, while extremely accurate in the case of a lossless, unforced spring of dimensions typical in spring reverberation units, is still lacking in several features which are necessary if one is to arrive at a complete model of a spring reverberation device.

Loss has not been considered here in any depth; as has been mentioned, models of loss in helical structures are not readily available. Even an empirical study of losses (by measuring, say, bandwithdths of spectral peaks, as in the case of a string of vibrating bar) is complicated, as there are two overlapping families of modal frequencies (corresponding to the two distinct dispersion relations for the system); furthermore, each mode is itself a mixture of longitudinal and transverse vibration, so a direct association with loss characteristics of simpler non-curved systems such as strings and bars is not immediately forthcoming.

The forcing mechanism also has not been described here. In a typical spring reverberation unit, the excitation is a permanent magnet attached to one end of the spring, and driven by an electromagnetic field (the strength of which is proportional to the input signal). The exact details of the forcing, and how it couples to the various components of displacement and rotation is as yet unknown, and is in need of experimental investigation. The analysis of boundary conditions for the spring system given in Section 2.4, however, does at least provide a framework for arriving at a compatible forcing term, which will certainly have the character of a mass-spring system.

The numerical method presented here is well-behaved numerically under all possible boundary terminations, which may be easily associated with those of the underlying model system; energy conservation, in the lossless case, has been used as a design principle. In terms of accuracy, however, other problems emerge—all are due to the appearance of a new length scale in the case of a tightly curved structure such as a spring found in a typical reverberation unit. The dispersion characteristics possess important features at relatively high wavenumbers (corresponding to the length of one turn of the helix); in uncoiled structures, such high wavenumbers are associated with high temporal frequencies, and

thus there is less perceptual importance associated with them. In this case, however, the temporal frequencies of interest lie directly in the low audio range, and thus great care is necessary in numerical design over the whole range of wavenumbers. One simple remedy is to operate at oversampled rates; but certain approaches based on parameterized FDTD methods (see Section A) offer some degree of control over such perceptually important features.

Given that the input and output locations for the spring reverberation system is generally always taken from the same locations (i.e., the ends of the spring), and also that the system is linear and time invariant, an interesting alternative to FDTD methods might involve modal approaches, as in, e.g., the standard helical spring literature [6], and also as used in sound synthesis [20, 21, 22]. The obvious advantages relative to FDTD methods are (a) reduced runtime cost, (b) the possibility of obtaining exact behaviour, and (c) better control over loss. There are disadvantages as well; one must precompute the modal shapes and frequencies offline, which is potentially a very large undertaking, as well as store them, for each new set of parameters d and μ, and for a particular set of boundary conditions; still, though, this would seem to be one of the most suitable systems for modal-based effects modeling.

A. IMPROVED FDTD DESIGNS

Numerical dispersion is a strong effect for the scheme presented in Section 3.3, which is the simplest possible choice for the helical spring system. Other choices are possible, including free parameters allowing for tuning of the algorithm. To this end, consider the following modifications of the spatial difference operators given in (25) and (27):

$$\mathbf{R}_d = \begin{bmatrix} -2\mu & 1-\mu^2+(1+\epsilon_1 h^2)\delta_{ss} \\ 1-\mu^2+(1+\epsilon_1 h^2)\delta_{ss} & 2\mu(1+(1+\epsilon_1 h^2)\delta_{ss}) \end{bmatrix}$$

$$\mathbf{A}_d = \begin{bmatrix} 1 & 0 \\ 0 & 1-(1+\epsilon_2 h^2)\delta_{ss} \end{bmatrix} \quad \mathbf{D}_d = \begin{bmatrix} 1 & 0 \\ 0 & d-(1+\epsilon_3 h^2)\delta_{ss} \end{bmatrix}$$

Three parameters ϵ_1, ϵ_2 and ϵ_3 have been introduced—note that all three are multiplied by factors of h^2, so that the resulting scheme (29), when the above operators are employed, remains consistent with the helical spring system [18].

Under appropriate choices of the free parameters (perhaps chosen through an optimization procedure), much better behaviour can be obtained at audio sample rates. See Figure 10. Interestingly, such schemes can also be cheaper computationally than the unparameterized scheme, as h_{min} is generally larger (leading to a smaller grid size).

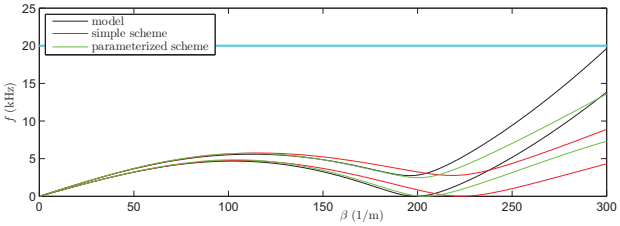

Figure 10: *Numerical dispersion relations, at 44.1 kHz, for a spring with $R = 5$ mm and $r = 1$ mm, and with pitch angle $\alpha = 5°$: for the simple scheme (in red) and for a parameterized scheme (in green), for $\epsilon_1 = 0.084$, $\epsilon_2 = -0.291$ and $\epsilon_3 = -0.364$.*

B. REFERENCES

[1] V. Välimäki, U. Zölzer, and J. O. Smith, Eds., 2010, IEEE Transactions on Audio Speech and Language Processing: Special Issue on Virtual Audio Effects and Musical Instruments.

[2] L. Hammond, "Electrical musical instrument," Feb. 2 1941, US Patent 2,230,836.

[3] A.C. Young and P. It, "Artificial reverberation unit," Oct. 8 1963, US Patent 3,106,610.

[4] J.D. Stack, "Sound reverberating device," Mar. 9 1948, US Patent 2,437,445.

[5] W. Wittrick, "On elastic wave propagation in helical springs," *International Journal of Mechanical Sciences*, vol. 8, pp. 25–47, 1966.

[6] J. Lee and D. Thompson, "Dynamic stiffness formulation, free vibration and wave motion of helical springs," *Journal of Sound and Vibration*, vol. 239, no. 2, pp. 297–320, 2001.

[7] V. Yildrim, "Investigation of parameters affecting free vibration frequancy of helical springs," *International Journal for Numerical Methods in Engineering*, vol. 39, pp. 99–114, 1996.

[8] L. Della Pietra and S. della Valle, "On the dynamic behaviour of axially excited helical springs," *Meccanica*, vol. 17, pp. 31–43, 1982.

[9] J. Abel, D. Berners, S. Costello, and J. O. Smith III, "Spring reverb emulation using dispersive allpass filters in a waveguide structure," 121st AES Convention, San Francisco, October, 2006. Preprint 6954.

[10] J. Parker, "Efficient dispersion generation structures for spring reverb emulation," *EURASIP Journal on Advances in Signal Processing*, vol. 2011, pp. 646134, 2011.

[11] J. Parker V. Välimäki and J. Abel, "Parametric spring reverberation effect," *Joural of the Audio Egineering Society*, vol. 58, no. 7/8, pp. 547–562, 2010.

[12] S. Bilbao and J. Parker, "A virtual model of spring reverberation," *IEEE Transactions on Audio Speech and Language Processing*, vol. 14, no. 2, pp. 695–705, 2010.

[13] K. Graff, *Wave Motion in Elastic Solids*, Dover, New York, New York, 1975.

[14] S. Bilbao and J. Parker, "Perceptual and numerical issues in spring reverberation models," in *Proceedings of the International Symposium on Musical Acoustics*, Sydney, Australia, 2010.

[15] S. Bilbao, *Numerical Sound Synthesis*, John Wiley and Sons, Chichester, UK, 2009.

[16] K. Yee, "Numerical solution of initial boundary value problems involving Maxwell's equations in isotropic media," *IEEE Transactions on Antennas and Propagation*, vol. 14, pp. 302–307, 1966.

[17] A. Taflove, *Computational Electrodynamics*, Artech House, Boston, Massachusetts, 1995.

[18] J. Strikwerda, *Finite Difference Schemes and Partial Differential Equations*, Wadsworth and Brooks/Cole Advanced Books and Software, Pacific Grove, California, 1989.

[19] B. Gustaffson, H.-O. Kreiss, and J. Oliger, *Time Dependent Problems and Difference Methods*, John Wiley and Sons, New York, New York, 1995.

[20] D. Morrison and J.-M. Adrien, "Mosaic: A framework for modal synthesis," *Computer Music Journal*, vol. 17, no. 1, pp. 45–56, 1993.

[21] J.-M. Adrien, "The missing link: Modal synthesis," in *Representations of Musical Signals*, G. DePoli, A. Picialli, and C. Roads, Eds., pp. 269–297. MIT Press, Cambridge, Massachusetts, 1991.

[22] L. Trautmann and R. Rabenstein, *Digital Sound Synthesis by Physical Modeling Using the Functional Transformation Method*, Kluwer Academic/Plenum Publishers, New York, New York, 2003.